Plasma Phys. Control. Fusion **42** (2000) 865–880. Printed in the UK PII: S0741-3335(00)11249-7

Direct comparison of experimental and theoretical results on the antenna loading and density jumps in a high pressure helicon source

Shunjiro Shinohara and Konstantin P Shamrai†

Interdisciplinary Graduate School of Engineering Sciences, Kyushu University, Kasuga, Fukuoka 816-8580, Japan

E-mail: sinohara@aees.kyushu-u.ac.jp

Received 21 January 2000, in final form 27 April 2000

Abstract. Operation modes of helicon discharge excited by double $m = 0$ antenna at high argon pressures of 51 and 6 mTorr are examined experimentally and theoretically. The behaviour of the discharge, including abrupt density jumps, is found to depend strongly on the relative directions of the currents in the antenna loops (on the antenna spectrum). Experimental results are interpreted in terms of theory which considers the radio frequency power absorption with due regard to the conversion of helicon waves into electrostatic waves. Computed dependences of the plasma load resistance on plasma density and input power, and magnetic field profiles satisfactorily agree with experimental data over a wide range of operation parameters. Thresholds for density jumps estimated from the power balance consideration are also in agreement with experimental values.

1. Introduction

Helicon discharge has attracted growing interest as a source of dense plasmas for various applications and basic research including materials processing, fusion experiments, gas lasers, modelling of space plasmas etc (see, e.g., [1, 2] and references therein). Both experiments and theoretical computations reported so far have normally dealt with discharges at relatively low gas pressures, in the range below 10–20 mTorr, when the electron collision frequency ν_e is less or about ω, the driving frequency. Note that in materials processing this pressure area is of primary interest for etching technologies [3]. Helicon plasmas demonstrate abrupt jumps between low and high density modes, which may be stimulated by a continuous variation of external parameters, for example, input power. These jumps are identified with transitions between three modes of antenna-to-plasma coupling, that is capacitively (CC), inductively (IC), and wave (WC) coupled modes. A CC to IC mode transition is intrinsic for any inductive discharge [4], whereas a transition between IC and WC modes is a characteristic feature of the helicon discharge. The latter was measured in experiments with various devices [5–7], and interpreted theoretically [8–11].

The area of high pressures, of the order of a few tens of mTorr, is of interest for deposition technologies [3]. For radio frequency (rf) sources, the electron collision frequency ν_e in this area is higher, or even much higher than ω. Normally, waves cannot propagate at such high

† Permanent address: Institute for Nuclear Research, 47 Prospect Nauki, Kiev 03680, Ukraine; e-mail: kshamrai@kinr.kiev.ua.

0741-3335/00/080865+16$30.00

collisions because of strong damping. However, this is not the case for helicon waves which are known to be weakly damped under condition $\nu_e \ll \omega_{ce} \cos\phi$, and thus can exist even at $\nu_e \gg \omega$ [12]. Here ω_{ce} is the electron cyclotron frequency, and ϕ the propagation angle with respect to the magnetic field. Although the capacity of the helicon discharge to operate at relatively high pressures, up to hundreds of mTorr, was reported in a set of experiments [13–15], little experimental data are available in this area.

In recent experiments [16], detailed measurements were performed on the discharge modes of a helicon source excited by double $m = 0$ antenna at a frequency of 7 MHz and high Ar pressures up to 51 mTorr. Depending on the electron density and temperature, the ν_e/ω ratio could reach the value of ten and more in those experiments. It was found that jump-like transitions, which increase the plasma density by up to two orders of magnitude, are intrinsic for the high pressure discharge as well as for the low pressure one. Density jumps are accompanied by jumps of the plasma load resistance, and by substantial alteration of the rf magnetic field profiles. The behaviour of the discharge was shown to depend strongly on the relative directions of the currents in the antenna loops, that is on the antenna spectrum.

In this paper, experimental data obtained in conditions similar to those of previous experiments [16] are compared in detail with computations on the basis of the theoretical model reported in [8]. That model takes into account, along with direct absorption of helicon waves due to collisions, the effect of mode conversion of helicons into electrostatic Trivelpiece–Gould waves. Obtained results, including the magnetic field profiles, dependences of plasma load resistance on plasma density and input power, and predictions of abrupt density jumps, are found to be in satisfactory agreement with experimental data over a wide range of operational parameters. The paper is organized as follows. A brief description of theoretical model and principal results for interpretations of experimental data are presented in section 2. Detailed comparison of experimental data with computations is made and discussed in section 3, followed by the concluding section, section 4.

2. Theoretical model and predictions

A theoretical model reported in [8] has been modified to perform computations for the experimental conditions [16]. A helicon source is considered as a uniform plasma column of radius r_0 restricted in the axial direction by two conducting flanges located at $z = R$ and L (see figure 1). The total length of the plasma column, $\Delta z = R - L$, makes a computation base. Two loops of the double $m = 0$ antenna, of radius r_a and of finite width d, contain currents which are equal in amplitude with parallel or anti-parallel directions. In the computations it is normally supposed that $r_0 = r_a$. A small gap between the plasma surface and antenna does not affect coupling substantially. One example in support of this statement will be given in figure 4 (see also [17]).

The density of the azimuthal antenna current, $j_a = i_a(z)\delta(r - r_0)\cos\omega t$, is represented as a sum of Fourier harmonics over axial discrete wavenumbers $k = l_z\pi/\Delta z$ ($l_z = 1, 2, \ldots$).

$$i_a = \sum i_k \sin kz' \tag{1}$$

where $z' = z - L$. The density of the antenna current is considered to be uniform across the antenna loops in the axial direction, the validity of this assumption being argued in [18]. In addition, it is supposed to be independent of the azimuthal angle, which corresponds to purely inductive (electromagnetic) coupling, $\nabla \cdot \boldsymbol{i}_a = 0$, that is in the absence of charges induced in the antenna. One can find the spectra i_k for the same and opposite directions of currents in the antenna loops in figure 2 of [16].

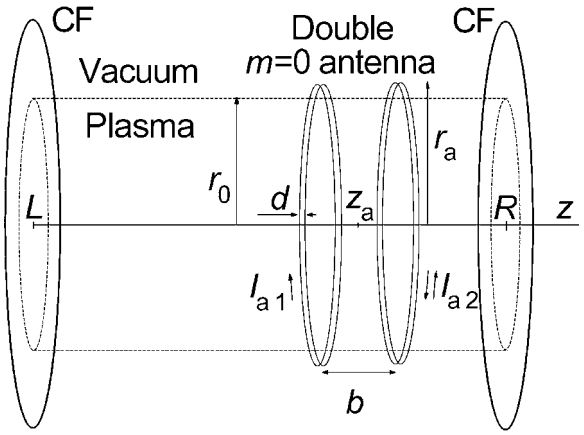

Figure 1. Theoretical model of a helicon source with conducting end flanges denoted as CF. Calculation parameters: $L = -80$ cm, $R = 0$ or 80 cm, $r_0 = 2.5$ cm, $z_a = -20$ cm, $b = 2$ cm, $d = 1$ cm, and $|I_{a1}| = |I_{a2}| = 1$ A.

Similar to (1) series are used to represent the fields:

$$\boldsymbol{E} = \sum \left[\boldsymbol{E}_{\perp k}(r)\sin kz' + \hat{\boldsymbol{z}}E_{zk}(r)\cos kz'\right]\exp(-\mathrm{i}\omega t) + \mathrm{cc} \tag{2}$$

$$\boldsymbol{B} = \sum \left[\boldsymbol{B}_{\perp k}(r)\cos kz' + \hat{\boldsymbol{z}}B_{zk}(r)\sin kz'\right]\exp(-\mathrm{i}\omega t) + \mathrm{cc} \tag{3}$$

where $\hat{\boldsymbol{z}}$ is a unit vector in the axial direction.

It is worth while noting that such an approach does not yield the total fields as purely standing in the z-direction waves. Each of the harmonics in expressions (2) and (3) is indeed the axially standing wave, but the total fields have standing patterns at zero dissipation only. In the presence of dissipation (collisions, Landau damping, etc), the spectral amplitudes of the fields are complex. As a result, sums (2) and (3) represent the fields with phases which depend on the axial coordinate as well as on the radial one. That means that total fields are not standing waves, but are found to be (outside the region under the antenna) the travelling waves, as irradiated by the antenna, with some standing admixture, due to partial reflection from the conducting ends. In the region under the antenna, fields have nearly standing patterns. Some travelling fraction may be found in this region due to the asymmetry of the antenna itself, or its position relative to the reflecting ends.

Series (2) and (3) are used to solve the Maxwell equations in the way described in [8]. Introducing the dimensionless field amplitudes $\boldsymbol{e}_k$ and $\boldsymbol{b}_k$

$$\boldsymbol{E}_k(r) = (2\pi/c)i_k\boldsymbol{e}_k(r) \qquad \boldsymbol{B}_k(r) = (2\pi/c)i_k\boldsymbol{b}_k(r) \tag{4}$$

one arrives at the following expression for the antenna load impedance $Z_a = R_a - \mathrm{i}L_a$

$$Z_a = -\frac{4\pi^2 r_0 \Delta z}{c}\sum\left|\frac{i_k}{I_a}\right|^2 e_{\theta k}(r = r_0) \tag{5}$$

where c is the speed of light, the sum is taken over all the harmonics, I_a is the amplitude of the antenna current, $e_{\theta k}$ is the complex amplitude of the azimuthal electric field, and cgs units are used. The plasma load impedance is defined as $Z_p = Z_a - Z_v$ where Z_v is the vacuum (without plasma) load impedance [8].

The dimensionless field amplitudes are the solutions to the following equations

$$\mathrm{i}Ne_{\theta k} = b_{rk} \qquad \mathrm{i}Nb_{\theta k} = K_1 e_{rk} + \mathrm{i}K_2 e_{\theta k}$$

$$N\left(e_{rk}-e'_{zk}\right)=\mathrm{i}b_{\theta k} \qquad N\left(b_{rk}+b'_{zk}\right)=K_2e_{rk}+\mathrm{i}K_1e_{\theta k}$$
$$\mathrm{i}N\left(\rho e_{\theta k}\right)'=-\rho b_{zk} \qquad \mathrm{i}N\left(\rho b_{\theta k}\right)'=\rho K_3e_{zk} \tag{6}$$

where $N=kc/\omega$ is a longitudinal refractive index, and the prime denotes a derivative with respect to the dimensionless radius $\rho=kr$. The permittivity tensor is considered in the following approximation (see, e.g. [19])

$$K_1=1-\left(\omega_{\mathrm{pe}}^2\gamma_{\mathrm{e}}/\Delta\right)-\left(\omega_{\mathrm{pi}}^2/\omega^2\gamma_{\mathrm{i}}\right) \qquad K_2=\omega_{\mathrm{pe}}^2\omega_{\mathrm{ce}}/\omega\Delta$$
$$K_3=1+(kr_{\mathrm{De}})^{-2}\left[1-w(\xi)\right]\left[1-\mathrm{i}(\nu_{\mathrm{e}}/\omega\gamma_{\mathrm{e}})w(\xi)\right]^{-1} \tag{7}$$

where $\omega_{\mathrm{pe,i}}$ are the electron and ion plasma frequencies, r_{De} is the electron Debye radius,

$$\Delta=(\omega\gamma_{\mathrm{e}})^2-\omega_{\mathrm{ce}}^2 \qquad \gamma_{\mathrm{e,i}}=1+\mathrm{i}(\nu_{\mathrm{e,i}}/\omega) \tag{8}$$

ω_{ce} is the electron cyclotron frequency, and it is assumed that $\omega\gg\omega_{\mathrm{ci}}$, the ion cyclotron frequency. Tensor (7) takes into account both electron–neutral and electron–ion collisions, with total frequency $\nu_{\mathrm{e}}=\nu_{\mathrm{en}}+\nu_{\mathrm{ei}}$, as well as ion collisions with frequency ν_{i}. We used in the computations the following approximation for electron–neutral collisions in argon, $\nu_{\mathrm{en}}=1.3\times10^6p_{\mathrm{Ar}}T_{\mathrm{e}}$ (s^{-1}), where p_{Ar} is the Ar pressure, in mTorr, and T_{e} the electron temperature, in eV. According to our calculations (see also [20]), this is a satisfactory estimation for the collision frequency in the range of electron temperatures of 3–8 eV. The electron–ion collision frequency, ν_{ei}, was estimated using the Spitzer formula. The ratio of $\nu_{\mathrm{ei}}/\nu_{\mathrm{en}}$ increases approximately linearly with electron density. For $n_0=10^{13}$ cm^{-3}, $p_{\mathrm{Ar}}=51$ mTorr, and $T_{\mathrm{e}}=4$ eV, this ratio makes the value of 0.15, whereas it is about unity at 6 mTorr. Ion–neutral collisions come into play at magnetic fields of the order of and above the critical value of 680 G, which is defined by the equation $\omega=\omega_{\mathrm{LH}}\approx(\omega_{\mathrm{ce}}\omega_{\mathrm{ci}})^{1/2}$, where ω_{LH} is the lower hybrid frequency, the ion cyclotron frequency ω_{ci} is estimated for Ar, and $\omega/2\pi=7$ MHz. For our conditions, the ratio of $\nu_{\mathrm{i}}/\nu_{\mathrm{e}}$ does not exceed 0.1, so that ion collisions are of minor importance for the wave damping.

The effect of Landau damping is included in the component K_3 of the permittivity tensor (7), where

$$\xi=\omega\gamma_{\mathrm{e}}/2^{1/2}k\nu_{\mathrm{Te}} \qquad w(\xi)=\pi^{1/2}\xi\exp(-\xi^2)[\mathrm{Erfi}(\xi)-\mathrm{i}] \tag{9}$$

ν_{Te} is the electron thermal velocity, and $\mathrm{Erfi}(\xi)$ the imaginary error function. This form of K_3 arises provided the collision integral is used in the Bhatnagar–Gross–Krook approximation [19]. That approximation is known to describe well the electron–neutral collisions, but it is not so adequate for Coulomb collisions. However, the use of K_3 in the above form (7) is adequately justified for two reasons. First, electron–ion collisions are substantially lower than electron–neutral collisions at the high pressures under consideration. Second, computations show the small effect of Landau damping, so that a more accurate treatment of the electron–ion collision integral is not needed.

Equations (6) should be completed by joining conditions at the plasma–vacuum interface $r=r_0$

$$\{\boldsymbol{e}_{\mathrm{t}}\}=\{e_z\}=\{\boldsymbol{b}_t\}=0 \qquad \{b_z\}=-1 \tag{10}$$

where braces refer to the boundary jump of appropriate variable, $\{f\}\equiv f(r_0+0)-f(r_0-0)$, and the subscript t denotes the field component tangential to the plasma surface.

We use the approximation of the uniform density profile, which seems to be quite relevant for our needs. Indeed, the effect of non uniformity is not so dramatic for $m=0$ excitation, as it is for $m=\pm1$ excitation. (In the latter case, the effect is enhanced due to the suppression of the $m=-1$ modes in non-uniform plasma [17, 21].) In addition, the profile is substantially

more uniform at high collisions as compared with the case of low collisions, as will be seen from figure 5 presented below.

With a uniform density profile, equations (6) and (10) are readily resolved in the Bessel functions [8]. Analysis of solutions obtained in this way show that rf power is absorbed via two different mechanisms. The first is direct absorption of helicon waves excited by antenna due to collisional and collisionless (Landau) damping [12]. The second mechanism, which is normally a dominant one, arises due to the edge conversion of helicon waves into electrostatic Trivelpiece–Gould (TG) waves [8]. Although TG waves are strongly damped at high collisions, the efficiency of this conversion mechanism turns out to be very high at $\nu_e > \omega$, as well as at $\nu_e < \omega$.

The obtained expressions for the fields and plasma load resistance were computed using the package Mathematica 3.0. A finite number of harmonics, $l_z = 1, 2, \ldots, l_{z\max}$, was taken into account in series (2), (3) and (5), with appropriate control of accuracy. In agreement with the experimental conditions [16], the numerical values of the geometrical parameters were chosen as follows (see figure 1)

$$z_a = -20 \text{ cm} \qquad b = 2 \text{ cm} \qquad d = 1 \text{ cm} \qquad r_0 = 2.5 \text{ cm} \qquad L = -80 \text{ cm}. \tag{11}$$

The position of the left-hand conducting flange in the computation model, $z = L = -80$ cm, is the same as in experiment [16]. To be strictly appropriate for the experiment, the axial position of the right-hand conducting flange should be chosen, generally speaking, at $z = R = 170$ cm. (In the experiment [16], the $z = 0$ position corresponds to the exit of the source into a large drift chamber of length 170 cm.) In this case, the total length of the plasma column (computation base) reaches the value of $\Delta z = 250$ cm. As long as a minimal axial scale, which is the width of antenna loops, reaches $d = 1$ cm, the number of harmonics to be taken into account, $l_{z\max}$, should be several times the ratio of $\Delta z/d$, that is several hundred. Such a scheme, however, takes too much time for computation. Fortunately, it was found that use of such a long computation base and large number of harmonics is not needed because of the considerable damping of helicon waves at high collisions. For calculations of the plasma load impedance, it was normally enough to put $R = 0$ cm, that is $\Delta z = 80$ cm, and to include $l_{z\max} = 50$ harmonics. Adding more harmonics, at the same base, did not change the result substantially. To check the accuracy we also computed the impedance with a longer base, $\Delta z = 160$ cm ($R = 80$ cm), and with increased number of harmonics, $l_{z\max} = 150$. The change in results was found to be less than 10%.

A higher number of harmonics and a longer computation base were needed to calculate the field profiles, especially in the area near the antenna. The problem is that very short-scale harmonics, corresponding to non-propagating (evanescenting) helicon waves, do not contribute to the absorption (see [8] for the justification), but they form the fine details of the near antenna field. It was found that $l_{z\max} = 300$ harmonics with $\Delta z = 160$ cm were enough to reach the accuracy of a few per cent.

Figure 2 shows the variation with density of real (resistance) and imaginary (reactance) parts of the plasma load impedance, $Z_p = R_p - iL_p$, calculated using relation (5). Note that $R_p = R_a$, as long as vacuum (without plasma) load resistance is neglected in theory. One can see from figure 2 that plasma resistance is not very sensitive to the electron temperature, and thus to the electron collision frequency, as well as to the effect of Landau damping. The effects of temperature and Landau damping on plasma reactance are higher at low densities, but decrease with increasing density.

In the low collision case, $\nu_e < \omega$, the variation of resistance with density and/or magnetic field is substantially non-monotonic [8]. This demonstrates a set of maxima and minima due to the contribution to the absorption of various axial and radial modes. At high collisions, the

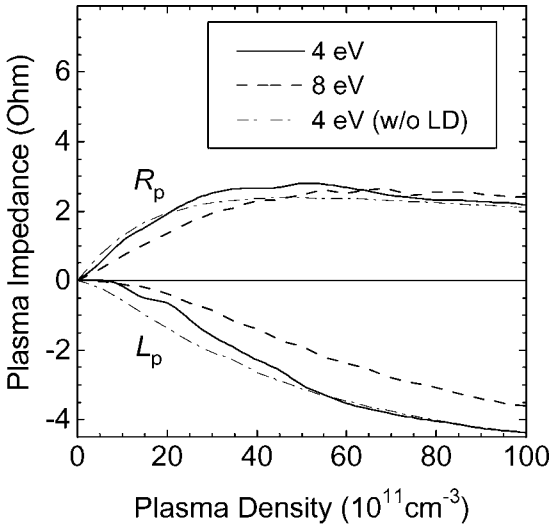

Figure 2. Computed variation with density of plasma load resistance (R_p) and reactance (L_p), for parallel currents in antenna loops. Magnetic field $B_0 = 100$ G and Ar pressure $p_{Ar} = 51$ mTorr. Three curves correspond to electron temperatures of 4 eV, 8 eV and 4 eV with Landau damping neglected.

variation of resistance is found to be quite smooth. As seen from a three-dimensional plot in figure 3, multiple maxima and minima are absent because they are blurred out by collisions at $p_{Ar} = 51$ mTorr. One can see from figure 3 that in the case of anti-parallel antenna currents the resistance reaches substantial values at low magnetic fields, and drops rapidly with increasing B_0. The reason for this is that the antenna excites only short helicon waves in this case (the first spectral maximum for anti-parallel currents is around $l_z \approx 35$). The threshold on density for the excitation of helicons [8],

$$n_0 > \frac{c}{8e}\frac{B_0 l_z^2}{f\,(\Delta z)^2} \tag{12}$$

where e is the electron charge, is found to be very high for short modes at high magnetic field. For $l_z = 35$ and $\Delta z = 80$ cm, inequality (12) takes the form $n_0 > 2.1 \times 10^{11} B_0$, where n_0 is in cm^{-3}, and B_0 in G. The resistance maximum at low B_0 is formed just as the result of the excitation of modes near the spectral maximum. In the region of $B_0 > 50$ G, the resistance is lower because it is formed by lower harmonics, $l_z < 35$, with relatively small amplitudes.

One can see from figure 3 that the calculated plasma resistance does not demonstrate any peculiarities in the range of magnetic fields relative to the lower hybrid resonance, $B_0 \approx 680$ G. The reason for this is that at high Ar pressures, $\nu_e > \omega$, the LH resonance is totally blurred out by collisions. This is in agreement with results on high pressure discharge [16] where no extra behaviour in the power absorption and density profiles was observed in the region of resonance magnetic fields.

In [8, 11], jumps of the helicon discharge to the high density mode were interpreted using the following power balance arguments. The power absorbed by the plasma takes the form $P_{abs}(n_0) = (1/2)R_p(n_0)I_a^2$, where $I_a = |I_{a1}| = |I_{a2}|$. With growing antenna current, the absorption curve, $P_{abs}(n_0)$, increases in amplitude. When the antenna current reaches some critical value, the absorption curve touches the loss line, $P_{loss} = \alpha n_0$, where α is some coefficient. Then the density jump occurs, as shown in figure 4. As long as our model takes

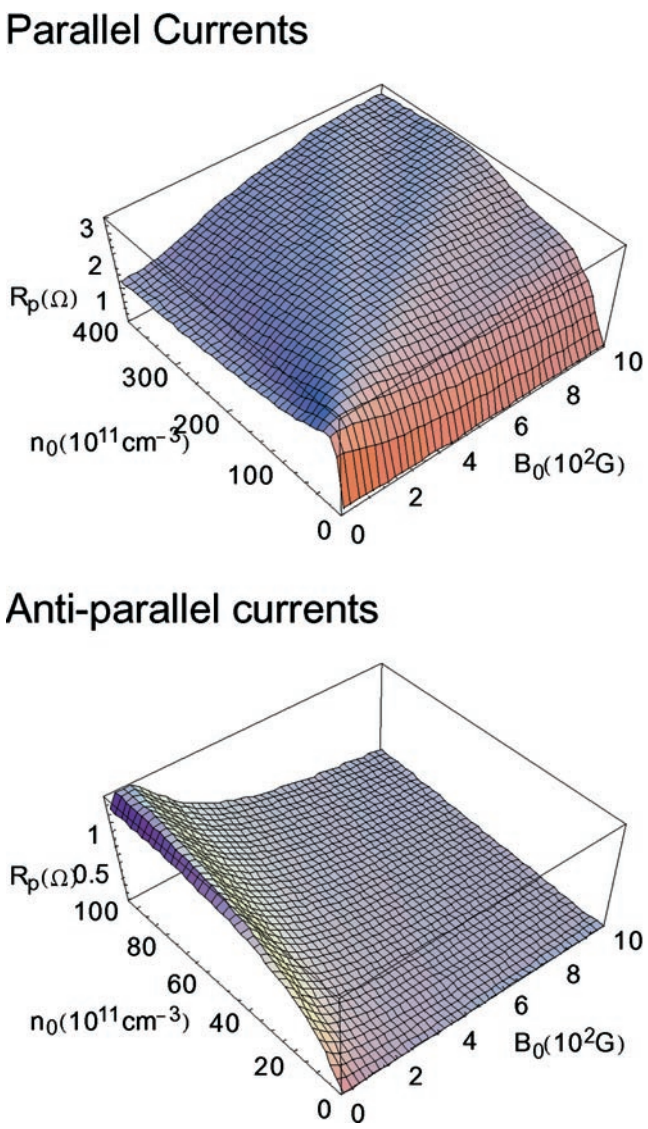

Figure 3. Computed dependences of plasma resistance on density and magnetic field, for parallel and anti-parallel antenna currents. $p_{Ar} = 51$ mTorr and $T_e = 4$ eV.
(This figure is in colour only in the electronic version, see `www.iop.org`)

into account inductive coupling only, it predicts that the discharge jumps from zero plasma density to $n_0 = n_{th}$. Of course, such an approach to the density jumps is substantially heuristic. It is based on the power balance arguments only, and does not specify the process of the jump in detail. A better understanding of that process needs a more perfect model with both rf power coupling and transport phenomena included, similar to that developed for modelling the rf plasma production in the magnetic trap in the ICR frequency range [22]. However, our simple approach turns out to yield reasonable estimations for jump thresholds.

To include the effect of the finite gap between the plasma column and antenna, one should multiply the terms of sum in the right-hand-side of formula (5) by $(r_a/r_0)[K_1(kr_a)/K_1(kr_0)]$

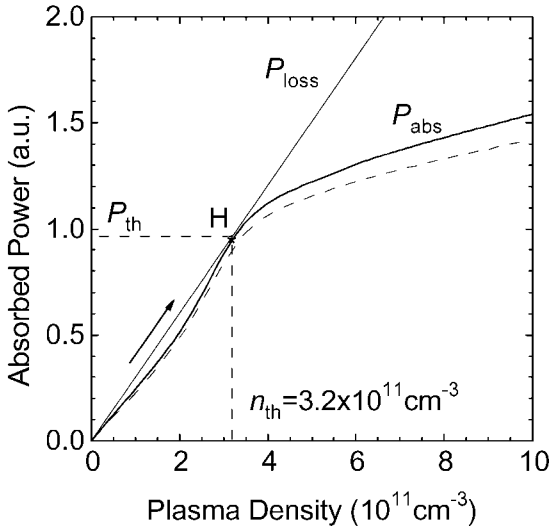

Figure 4. Absorption curve (full curve) at a critical antenna current corresponding to the coupling of the discharge to the high mode of density $n_{\rm th}$. The jump to the point H, shown by an arrow, occurs at a critical absorbed power $P_{\rm th}$. A straight line shows the plasma losses assumed to depend linearly on density, $P_{\rm loss} = \alpha n_0$. Calculation parameters: parallel antenna currents, $p_{\rm Ar} = 6$ mTorr, and $T_{\rm e} = 8$ eV. The broken absorption curve was computed with a finite gap between the antenna and plasma, at $r_{\rm a} = 3$ cm.

where K_1 is the Macdonald function. The broken curve in figure 4 was computed with an antenna 0.5 cm from the plasma, $r_{\rm a} = 3$ cm. One can see that the effect of the vacuum gap is very small at low densities but increases with density, the reason for this being as follows. In a vacuum, perpendicular wavenumbers of harmonics generated by antenna are $k_\perp \approx {\rm i}k\ \left(N^2 + N_\perp^2 = 1,\ N \gg 1\right)$, so that their fields drop from the antenna approximately as $\exp(-k|r - r_{\rm a}|)$. Long harmonics easily penetrate through the vacuum gap to excite fields in the plasma, whereas short harmonics, which satisfy the inequality

$$k(r_{\rm a} - r_0) > 1 \tag{13}$$

are substantially reduced in the plasma. The effect of the gap depends on how many harmonics satisfying (13) are included in the antenna spectrum, and on how effectively these harmonics are excited in the plasma. The role of short harmonics is clearly more important in the spectrum of anti-parallel currents. On the other hand, the excitation of short harmonics in the plasma is more effective at high densities, as seen from relation (12). Computations show that a reduction of impedance due to the 0.5 cm vacuum gap turns out to be less than 30% over the range of densities under consideration. As long as thresholds for jumps are estimated at relatively low densities, the presence of the gap is of minor importance for these values, as seen from figure 4.

The above theoretical approach was used for computations of the wave patterns and rf power absorption in various conditions relative to experiment, and for estimations of thresholds for abrupt density jumps. The results of comparison with experiment are presented in the next section.

3. Comparison of experimental and theoretical results

Experiments were performed with a 5 cm diameter source attached to a 170 cm long drift chamber [5, 16, 8]. The length of the discharge tube outside the chamber was 80 cm. The

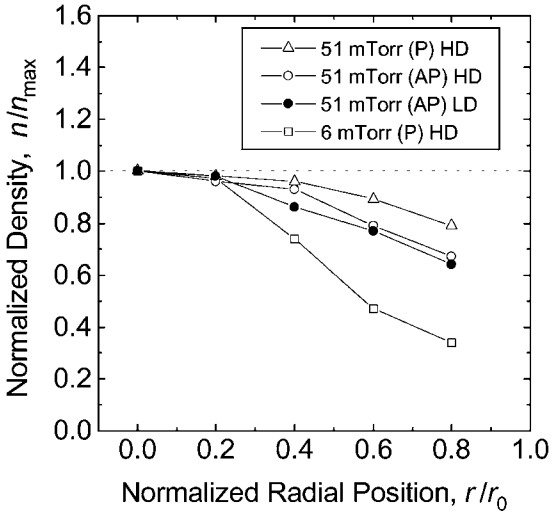

Figure 5. Radial density profiles for various discharge regimes at Ar pressures of 51 mTorr (100 G) and 6 mTorr (500 G). P and AP refer to the parallel and anti-parallel directions of currents in antenna loops. HD and LD denote the high density mode (in the range of 10^{13} cm^{-3}) and low density mode (in the range of 10^{11} cm^{-3}).

discharge was excited at a frequency of $\omega/2\pi = 7$ MHz by double $m = 0$ antenna, both at the same and opposite directions of currents in antenna loops. The electron collision frequency $\nu_e \gg \omega$ at a working Ar pressure of 51 mTorr; $\nu_e \approx \omega$ at 6 mTorr. Data were taken over a wide range of magnetic fields, 0 to 1000 G, and input powers up to 2500 W. It was found that at high Ar pressures the variation of plasma density with input power demonstrates abrupt density jumps, as well as at low pressures [5]. The high density mode in the range of 10^{13} cm^{-3} could be attained at input powers of 100 to 1000 W, depending on the magnetic field, relative directions of the currents in the antenna loops, and gas pressure. Detailed measurements were conducted of the antenna loading resistance, which also demonstrates jumps, and of axial and radial profiles and phases of the magnetic field. Antenna loading was defined as input power, P_{in}, divided by the square of the effective antenna current. P_{in} is the difference between the incident and reflected power derived by a directional coupler, and there were monitors for the antenna voltage and current. An accuracy of the antenna load resistance obtained in this way including reproducibility is estimated to be about 10–20%. Experimental results, which are partly presented in [16], are compared below with computations.

The relevance of the results computed in the uniform plasma approximation is justified by the fact that the radial density profile in helicon discharge is much more uniform at high pressures than it is at low pressures. Figure 5 shows several profiles measured for various regimes. One can see that decrease of density at $r = 0.8r_0 = 2$ cm is less than 40% relative to the central density, at a high pressure of 51 mTorr and magnetic field of 100 G. Note that profiles are very similar both in the high and low density modes for anti-parallel currents in antenna loops. The profile tends to be more peaked with increasing magnetic field and decreasing pressure. This tendency can be seen from figure 5, where the density profile is substantially more non uniform at 6 mTorr and 500 G.

To compare the experimental and theoretical results, we consider below, preferentially, experimental regimes with a relatively high degree of plasma uniformity. Although the plasma density just near the edge was not measured in these regimes, it is supposed to be high enough

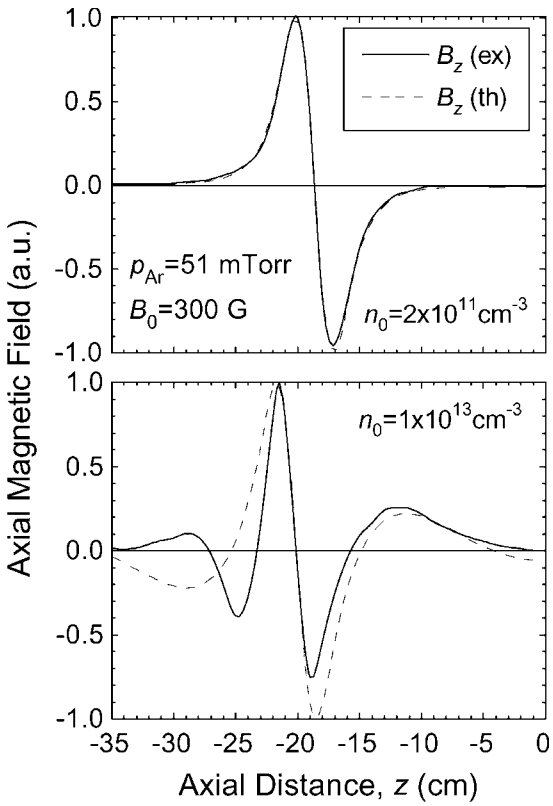

Figure 6. Comparison of experimental and theoretical axial profiles of the $B_z(r = 0)$ magnetic field excited with anti-parallel currents in antenna loops. The top and bottom figures correspond to the low density (before the jump) and high density (after the jump) modes, at $p_{\rm Ar} = 51$ mTorr and $B_0 = 300$ G.

to give rise to a substantial absorption via edge mode conversion, the efficiency of which is roughly proportional to the edge density [23]. At low edge density, the surface conversion is reduced [17, 24], but then the bulk mode conversion provides the efficient absorption. Note that agreement of our experimental and theoretical results is found to be not so poor even at reduced radial uniformity.

Figure 6 shows the experimental and computed axial profiles of the B_z field excited by the double-loop antenna with opposite directions of current, before and after the density jump in discharge at $p_{\rm Ar} = 51$ mTorr and $B_0 = 300$ G. The radial density profiles in both high and low density modes are similar to those plotted in figure 5 for the same conditions but $B_0 = 100$ G. Computations were carried out with the base $\Delta z = 160$ cm and using $l_{z\,\max} = 300$ harmonics. One can see from figure 6 that in low density mode, at $n_0 = 2 \times 10^{11}$ cm^{-3}, the antenna excites the evanescenting field. The agreement of theory with experiment is pretty good in this case, so that the measured magnetic field may be attributed to the excitation via purely inductive coupling. In the high density mode, at $n_0 = 1 \times 10^{13}$ cm^{-3}, theory also yields a proper profile to the right from the antenna, but the agreement is poor to the left. Such a disagreement is thought to arise from distortions due to the probe pipe. In the experiment, the pipe is inserted through a remote end flange located at $z = 170$ cm and goes along the axis to the left, with special care taken to keep the probe at the axis (see details in [16]). While the probe is to the

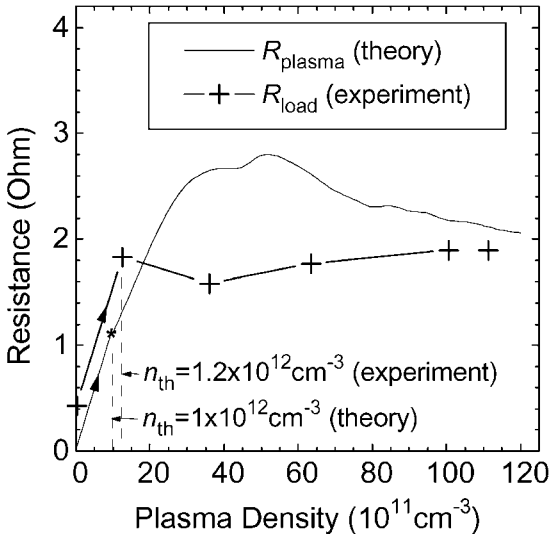

Figure 7. Comparison of experimental and theoretical dependences on density of the plasma load resistance for parallel antenna currents. Arrows show the density jumps. Both experimental and theoretical values of the threshold density (just after the jump) are shown. $p_{Ar} = 51$ mTorr and $B_0 = 100$ G. In calculations, it is assumed that $T_e = 4$ eV.

right relative to the antenna position, $z > z_a \approx -20$ cm, it disturbs the plasma only slightly. But when the probe head crosses the antenna region, the probe pipe introduces quite strong disturbances because it causes the E_z field to vanish at the axis, which is not compatible with $m = 0$ excitation. Although the E_z field is quite weak as compared with other components, the disturbances could be so strong in some regimes as to result in breaking the discharge down when the probe head passes through the antenna region. One more piece of evidence for the strong disturbances induced by the probe is that the experimental B_z profile in the bottom of figure 6 is highly non-antisymmetric relative to the antenna midplane. As seen from figure 6, theory predicts a slightly deeper penetration of the field into the downstream plasma, that is a slightly higher level of irradiated waves (wave coupling). A probable reason for that is the uniform plasma approximation.

Comparison of measured and computed load resistances is presented in figure 7, for $p_{Ar} = 51$ mTorr, $B_0 = 100$ G, and parallel antenna currents. Experimental points are plotted versus values of density measured at the discharge centre at $z \approx -22$ cm. Theoretical prediction of jump is based on the above discussed arguments (see figure 4). One can see from figure 7 a good agreement between the experimental value of threshold density (just after the jump), $n_{th} = 1 \times 10^{12}$ cm^{-3}, and that predicted by theory, $n_{th} = 1.2 \times 10^{12}$ cm^{-3}. At $n_0 > 2 \times 10^{12}$ cm^{-3}, theory predicts the resistance to be higher than the experimental value by a factor of about 1.5. Theoretical and experimental dependences in figure 7 are closer at higher densities, around 1×10^{13} cm^{-3}. The improvement of agreement may result from the fact that the plasma is radially very uniform at high densities, as seen from figure 5.

When comparing theoretical and experimental values of resistance in figure 7 and in the following figures 8–12, one must bear in mind that calculated the resistance corresponds to the net plasma absorption, whereas the measured resistance also includes the non-plasma part. The latter is defined by losses in the circuitry and by those dissipated by currents induced in the metal environment (end-flanges, magnetic coils, probes, etc). In the absence of plasma,

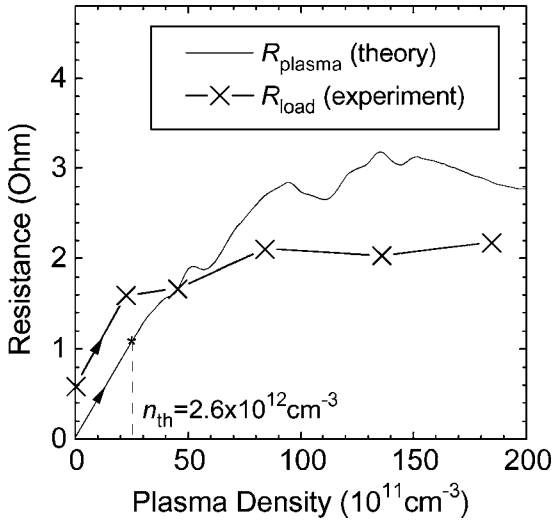

Figure 8. The same as in figure 7, but at $B_0 = 300$ G. Experimental threshold density $n_{th} = 2.4 \times 10^{12}$ cm^{-3} (not shown).

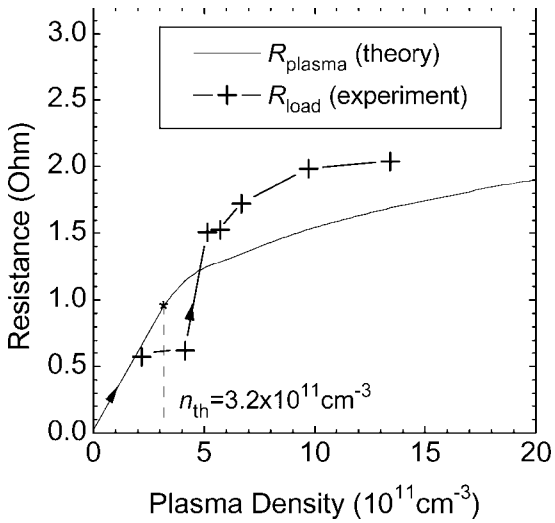

Figure 9. The same as in figure 7, but at $p_{Ar} = 6$ mTorr. Experimental threshold density $n_{th} = 5.1 \times 10^{11}$ cm^{-3} (not shown).

the value of non-plasma losses reaches 0.4–0.5 Ω [16], but this value is not well defined in the presence of plasma. Indeed, the plasma gives rise to substantial changes of fields in the neighbourhood of the metal environment, and thus to changes of the appropriate parts of non-plasma losses. To get the experimental value of net plasma resistance, one must certainly reduce the measured load resistance by a few tenths of an ohm, but the exact amount to be subtracted is not known.

Figure 8 shows computed and measured resistances for $p_{Ar} = 51$ mTorr, $B_0 = 300$ G, and parallel antenna currents. One can see that, similarly to the previous case, threshold densities for jump are very close in theory and experiment, and the agreement of resistances is satisfactory

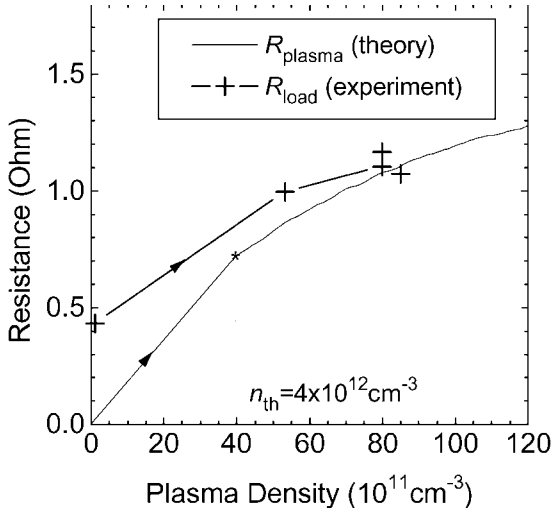

Figure 10. The same as in figure 7, but for anti-parallel currents in the antenna loops. Experimental threshold density $n_{\rm th} = 5.3 \times 10^{12}$ cm^{-3} (not shown).

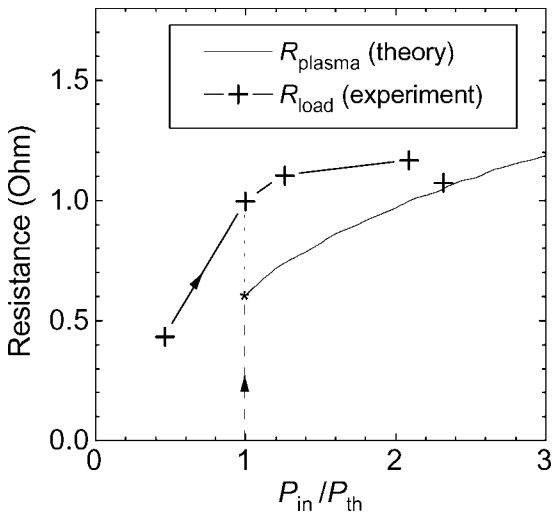

Figure 11. Comparison of experimental and theoretical dependences on input power of the plasma load resistance for anti-parallel antenna currents. The arrows show the density jumps. $p_{\rm Ar} = 51$ mTorr and $B_0 = 100$ G. The theoretical curve was computed at $T_{\rm e} = 4$ eV.

over all the range of densities. The agreement does not improve at high densities because measured radial non-uniformity is higher than it was in the previous case of $B_0 = 100$ G.

As can be seen from figure 9, the agreement between threshold densities is within 50% for the lower Ar pressure of 6 mTorr. Experimental resistance, if reduced by circuitry losses, is quite well fitted to the theoretical curve over all the range of densities. This is in spite of the fact that the measured density is radially very non uniform in this case, so that resistance computed in the uniform model is expected to exceed the experimental value. For $p_{\rm Ar} = 51$ mTorr, $B_0 = 100$ G, and anti-parallel antenna currents, threshold densities agree within 30%, and computed values of the resistance are close to the experimental ones (see figure 10). This is as

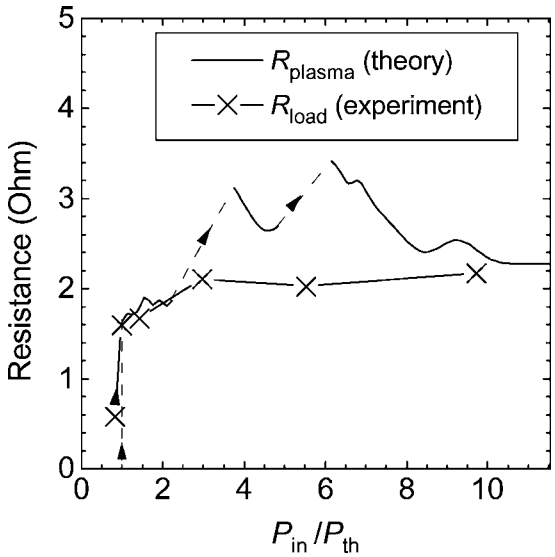

Figure 12. The same as in figure 11, but for parallel antenna currents and $B_0 = 300$ G. Broken curves with arrows show the three density jumps predicted by theory.

expected, because the measured density is quite uniform, as seen from figure 5. One can see from figures 7–10 that both experiment and computation show the tendency of the threshold density to increase with magnetic field and gas pressure. Thresholds for jumps turn out to be higher with the use of anti-parallel currents, which excite shorter waves. This tendency is in agreement with (12).

We also compared the experimental and theoretical dependences of plasma resistance on input power. As long as plasma losses are not specified in our model, the absolute value of the absorbed power is also not specified. For this reason, we use for comparison the values of input power, for experiment, and absorbed power, for theory, both normalized by threshold powers for the density jump, P_{th}. Figure 11 shows the plasma resistance versus normalized power for the same conditions as in figure 10. The variation of resistance with power is smooth after a jump. The plot in figure 12 is for the same conditions as in figure 8. As long as the dependence of resistance on density turns out to be non-monotonic in this case, theory predicts two additional jumps within the high density mode. However, it is not clear whether these jumps could be observed in the experiment.

Predictions of density jumps were based on the assumption that plasma losses in the discharge scale linearly with density, $P_{loss} = \alpha n_0$. That assumption was theoretically justified in [13] for radial losses, which are expected to be dominant in a long discharge at high pressures. To verify if it is so in our experiments, we plotted in figure 13 a number of experimental points for the discharge at $p_{Ar} = 51$ mTorr in various regimes. As can be seen, the variation of density with input power is nearly linear in the high density mode ($n_0 > n_{th}$, $P_{in} > P_{th}$). That means that losses are also linear with density, as a result of the balance condition, $P_{in} = P_{loss}$. The only well scattered point in figure 13 is related to very high input power, when the nonlinear effects are expected to be important.

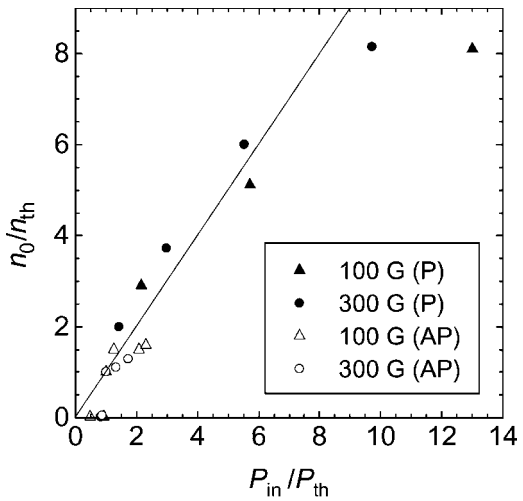

Figure 13. Experimental data on normalized plasma density against input power, for various discharge modes and conditions. The full line corresponds to $n_0/n_{th} = P_{in}/P_{th}$. P and AP refer to the parallel and anti-parallel directions of currents in the antenna loops.

4. Conclusion

A gradual increase of input power stimulates an abrupt density jump in helicon discharge at high Ar pressures ($\nu_e \gg \omega$) as well as at low pressures ($\nu_e \leqslant \omega$). Thresholds for jumps on power and density increase with magnetic field and gas pressure. They are also higher with anti-parallel currents in antenna loops, when axially short waves are excited. This gives, in principle, the possibility of controlling a discharge by the antenna spectrum. Density jumps are accompanied by jumps of the plasma load resistance, and by change of the field profiles. At low densities, in the range of 10^{10}–10^{11} cm^{-3}, a magnetic field is formed by non-propagating modes, and is axially monotonically evanescenting over a few centimetres from the antenna. This is supposed to result from the inductive coupling of the antenna to the plasma. In the high density mode, in the range of 10^{12}–10^{13} cm^{-3}, fields penetrate deeper into a downstream plasma, and have oscillating profiles. This implies that low damped helicon waves exist at the high pressures under consideration, and can support the wave coupling of the antenna to the plasma.

A quite simple model, which supposes a uniform density profile and thus takes into account the mode conversion of helicon waves into electrostatic TG waves at the plasma edge [8], turns out to satisfactorily explain the experimental results. (Note that at high pressures, $\nu_e > \omega$, strongly damping TG waves are in fact evanescenting oscillations which exist in our model near the plasma edge only.) Computed results were found to depend only slightly on electron temperature (and thus on collision frequency, since $\nu_e \approx \nu_{en} \propto T_e$), and to be practically independent of Landau damping. Theory yields the profiles of the magnetic field in a satisfactory agreement with the experiment. It also explains, on the average, to within a factor of 1.5, dependences of plasma load resistance on plasma density and input power. Using the power balance arguments permits one to interpret abrupt density jumps in discharge. Theory predicts a true tendency for jump thresholds, both on density and input power, to increase with the increase of the magnetic field and gas pressure, and with shortening the wavelengths excited by the antenna. Computed and experimental values of thresholds agree to within 50%.

A better agreement is expected when the effect of radial plasma non-uniformity is included in the theory. For various modes of high pressure discharge we also examined the relation between inductive and wave coupling, as well as the relative role in absorption of helicon and TG waves, and will present the results elsewhere.

Acknowledgments

One of the authors (KPS) is grateful for the hospitality of members of the laboratory of Professor Y Kawai. His continuous encouragement of this work is appreciated. KPS acknowledges with thanks the support of his visit to Kyushu University by the Venture Business Laboratory.

References

[1] Boswell R W and Chen F F 1997 *IEEE Trans. Plasma Sci.* **25** 1229
[2] Chen F F and Boswell R W 1997 *IEEE Trans. Plasma Sci.* **25** 1245
[3] Hershkowitz N 1998 *IEEE Trans. Plasma Sci.* **26** 1610
[4] Hopwood J 1992 *Plasma Sources Sci. Technol.* **1** 109
[5] Shinohara S, Miyauchi Y and Kawai Y 1995 *Plasma Phys. Control. Fusion* **37** 1015
[6] Ellingboe A R and Boswell R W 1996 *Phys. Plasmas* **3** 2797
[7] Blackwell D D and Chen F F 1997 *Plasma Sources Sci. Technol.* **6** 569
[8] Shamrai K P, Pavlenko V P and Taranov V B 1997 *Plasma Phys. Control. Fusion* **39** 505
[9] Kwak J G, Choi H D, Bak H I, Cho S, Bak J G and Kim S K 1997 *Phys. Plasmas* **4** 1463
[10] Mouzouris Y and Scharer J E 1998 *Phys. Plasmas* **5** 4253
[11] Shamrai K P 1998 *Plasma Sources Sci. Technol.* **7** 499
[12] Chen F F 1991 *Plasma Phys. Control. Fusion* **33** 339
[13] Chen F F 1992 *J. Vac. Sci. Technol.* A **10** 1389
[14] Mieno T, Shoji T and Kadota K 1992 *Japan. J. Appl. Phys.* **31** 1879
[15] Tynan G R *et al* 1997 *J. Vac. Sci. Technol.* A **15** 2885
[16] Shinohara S and Yonekura K 2000 *Plasma Phys. Control. Fusion* **42** 41
[17] Arnush D and Chen F F 1998 *Phys. Plasmas* **5** 1239
[18] Shinohara S, Kaneda N and Kawai Y 1998 *Thin Solid Films* **316** 139
[19] Ginsburg V L and Rukhadze A A 1975 *Volny v Magnitoaktivnoy Plazme* (Moscow: Nauka) (in Russian) (Engl. Transl. *Waves in Magnetized Plasmas*)
[20] Stevens J E, Sowa M J and Cecchi J L 1995 *J. Vac. Sci. Technol.* A **13** 2476
[21] Krämer M 1999 *Phys. Plasmas* **6** 1052
[22] Moiseenko V E, Plyusnin V V, Lyssoivan A I, Volkov E D, Nazarov N I, Kasilov S V and Litvinov A P 1996 *Proc. 23rd EPS Conf. on Control. Fusion and Plasma Phys. (Kiev, 1996)* vol 20C (Geneva: EPS) part II, p 926
[23] Shamrai K P 1999 *Fizika Plazmy* **25** 934 (Engl. Transl. *Plasma Phys. Rep.* **25** 860)
[24] Enk Th and Krämer M 1999 *Preprint* 74-A12-99, Institut für Experimentalphysik II, Ruhr-Universität Bochum